Temporal interpolation of land surface fluxes derived from remote sensing - results with an Unmanned Aerial System

Sheng Wang[1], Monica Garcia[1,2], Andreas Ibrom[1], Peter Bauer-Gottwein[2]

[1]Department of Environmental Engineering, Technical University of Denmark, 2800 Kgs. Lyngby, Denmark
5 [2]International Research Institute for Climate and Society, The Earth Institute, Columbia University, Palisades, NY, USA

Correspondence to: Sheng Wang (shengwang12@gmail.com), Monica Garcia (mgarc@env.dtu.dk)

Abstract. Remote sensing imagery can provide snapshots of rapidly changing land surface variables, e.g. evapotranspiration (ET), land surface temperature (T_s), net radiation (Rn), soil moisture (SM) and gross primary productivity (GPP), for the time of sensor overpass. However, discontinuous data acquisitions limit the applicability of remote sensing for water resources and
10 ecosystem management. Methods to interpolate between remote sensing snapshot data and to upscale them from instantaneous to daily time scale are needed. We developed a dynamic Soil Vegetation Atmosphere Transfer model to interpolate land surface state variables that change rapidly between remote sensing observations. The Soil-Vegetation, Energy, water and CO_2 traNsfer model (SVEN), which combines the snapshot version of the remote sensing Priestley Taylor Jet Propulsion Laboratory ET model and light use efficiency GPP models, incorporates now a dynamic component for the ground heat flux based on the
15 'force-restore' method and a water balance bucket model to estimate SM and canopy wetness at half-hourly time step. A case study was conducted to demonstrate the method using optical and thermal data from an Unmanned Aerial System in a willow plantation flux site (Risoe, Denmark). Based on model parameter calibration with the snapshots of land surface variables at the time of flight, SVEN interpolated the snapshot T_s, Rn, SM, ET and GPP to continuous records for the growing season of 2016 with forcing from continuous climatic data and NDVI. Validation with eddy covariance and other in-situ observations
20 indicates that SVEN can well estimate daily land surface fluxes between remote sensing acquisitions with root mean square deviations of the simulated daily T_s, Rn, SM, LE and GPP equal to 2.35 °C, 14.49 W·m^{-2}, 1.98% m^3·m^{-3}, 16.62 W·m^{-2} and 3.01 g·C·m^{-2}·d^{-1}, respectively. This study demonstrates that, in this deciduous tree planation, temporally sparse optical and thermal remote sensing observations can be used as "ground truth" to calibrate soil and vegetation parameters of a simple land surface modelling scheme to estimate "low persistence" or rapidly changing land surface variables with the use of few forcing
25 variables. This approach can also be applied with remotely sensed data from other platforms to fill temporal gaps, e.g. cloud induced data gaps in satellite observation.

1 Introduction

Continuous estimates of the coupled exchanges of energy, water and CO_2 between the land surface and the atmosphere are essential to understand ecohydrological processes (Jung et al., 2011), to improve agricultural water management (Fisher et al.,

2017), and to inform policy decisions for societal applications (Denis et al., 2017). Earth observation (EO) data have been increasingly used to estimate the land surface-atmosphere flux exchanges at the time of sensor overpass with minimum parameterization, particularly for regions with scarce ground observations. Optical and thermal remote sensing can provide snapshots of these fluxes such as soil moisture (SM) (Carlson et al., 1995; Sandholt et al., 2002), evapotranspiration (ET)

5 (Fisher et al., 2008; Mu et al., 2013) or gross primary productivity (GPP) (Running et al., 2004) using land surface reflectance or temperature. However, both optical and thermal satellite observations present gaps during cloudy periods, and those gaps may coincide with the time when such information is mostly needed (Westermann et al., 2011), for instance the high frequency of cloudy weather during the crop growing season in monsoonal regimes (García et al., 2013) and high latitude regions (Wang et al., 2018a). Methods are needed to temporally interpolate and upscale the instantaneous records into continuous daily,

10 monthly or annual values (Alfieri et al., 2017; Huang et al., 2016). As one of the most exciting recent advances in near-Earth observation, Unmanned Aerial Systems (UAS) can flexibly fly at a low altitude (< 100-200 m) with favourable revisit times and low cost (Berni et al., 2009; McCabe et al., 2017). Compared to satellites, UAS provide opportunities to acquire high temporal and spatial resolution data under cloudy weather conditions to monitor and understand the surface-atmosphere energy, water and CO_2 fluxes. However, UAS observations still just provide snapshots of the land surface status at the time of

15 the flight, while conditions such as land surface temperature (T_s), net radiation (Rn), SM, ET and GPP between image acquisitions remain uncovered.

To continuously estimate land surface-atmosphere energy, water and CO_2 fluxes, remote sensing based observations or simulations require either statistical or process-model based approaches to be interpolated into continuous records. The statistical approach is often used to interpolate those land surface variables with low persistence, e.g., which do not change

20 rapidly and can be assumed to be static during several days. For instance, to exclude cloud influence for proxies of vegetation structure e.g. vegetation indices (VI), satellite products use pixel composites to take the maximum value of VI from a given period between 8 and 16 days. To fill the gaps for this period, these 8 or 16 day maximum VI can be statistically interpolated into daily or sub-daily time series data, as the vegetation growth does not change significantly during such a short period. However, for variables that change substantially at sub-daily or daily time scales in response to changes in the surface energy

25 balance, e.g. T_s, Rn, SM, ET and GPP, using statistical interpolation could be challenging with low revisit frequency. For instance, Alfieri et al. (2017) found that a return interval of EO observations of no less than 5 days was necessary to statistically interpolate daily ET with relative errors smaller than 20%. To interpolate low persistence variables between remote sensing acquisitions, a dynamic model based interpolation approach considering the dynamics of the land surface energy balance can be better.

30 Ecosystem and land surface models, which can be used to diagnose and predict ecosystem functioning in a variable climatic conditions, such as BIOME-BGC (Running and Coughlan, 1988) and Simple Interactive Biosphere Model (SiB2, Sellers et al., 1996), can be used to temporally interpolate the land surface fluxes between EO snapshots with available model drivers and parameter values. Djamai et al. (2016) combined Soil Moisture Ocean Salinity (SMOS) Disaggregation, which is based

on the Physical and Theoretical Scale Change (DisPATCh) downscaling algorithm, with the Canadian Land Surface Scheme (CLASS) to temporally interpolate SM at very high spatial and temporal resolutions. Malbéteau et al. (2018) used the ensemble Kalman filter approach to assimilate DisPATCh into a simple dynamic model to temporally interpolate SM. Jin et al. (2018) temporally interpolated AMSR-E based SM estimates with the China Soil Moisture Dataset (SCMD) from the Microwave

5 Data Assimilation system. However, temporal interpolation using complex land surface models requires large data inputs and complicated parameterization schemes, as for example the turbulent fluxes are typically modelled using mass-transfer approaches. In view of these challenges, simpler but operational models based interpolation can be derived for snapshot remote sensing models of land surface variables. For instance, using a one-dimensional heat transfer equation, Zhang et al. (2015) interpolated the daily T_s on cloudy days. Based on surface energy balance (SEB), Huang et al. (2014) proposed a generic

10 framework with two to twelve parameters to temporally interpolate satellite based instantaneous T_s to diurnal temperatures for the clear sky conditions with mean absolute errors from 1.71 to 0.33 °C, respectively. However, model based approaches to temporally interpolate various land surface fluxes such as ET and GPP are rare.

This study aims at developing a simple but operational land surface modeling scheme, which simulates the land surface energy balance and water and CO_2 fluxes between the land surface and the atmosphere. We aimed at using EO based prescribed

15 vegetation dynamics from vegetation indices, limited meteorological inputs and parameters which can be optimized from remote sensing derived fluxes. It can be used for various conditions even in data scarce regions by performing parameter calibration with snapshot remote sensing estimates of T_s, SM, ET or GPP at the time of overpass. A Soil-Vegetation water and CO_2 flux Exchange, eNergy balance model (SVEN) was developed to continuously estimate T_s, SM, GPP and ET. The SVEN model is based on a joint ET and GPP model, which combines a light use efficiency GPP model and the Priestley–Taylor Jet

20 Propulsion Laboratory ET model (Wang et al., 2018a). This joint ET and GPP diagnostic model can simulate canopy photosynthesis, evaporation of intercepted water, transpiration and soil evaporation with EO data as inputs. This model now becomes a part of the transient surface energy balance scheme, SVEN, which incorporates additional processes and interactions between soil, vegetation and atmosphere, e.g. surface energy balance, sensible heat flux, and SM dynamics, to be able to simulate the land surface fluxes when EO data are not available. Compared to most traditional land surface models, which

25 couple processes of transpiration and CO_2 exchange through stomata behaviour and use a 'bottom-up' approach to upscale processes from the leaf scale to the canopy scale (Choudhury and Monteith, 1988; Shuttleworth and Wallace, 1985), SVEN uses a 'top-down' approach to directly simulate water and CO_2 fluxes at the canopy scale. SVEN estimates GPP and ET under potential or optimum conditions and then the potential values are down-regulated by the same biophysical constraints reflecting multiple limitations or stresses. These constraints can be derived from remote sensing and atmospheric data (García et al.,

30 2013; McCallum et al., 2009). In this way, SVEN avoids detailed descriptions and parameterization of complex radiation transfer processes at the leaf level and the scaling process to canopy level. It maintains a level of complexity comparable to that of operational remote sensing based GPP and ET instantaneous models while being able to predict the fluxes in periods without EO data.

The main objective of this study was to demonstrate a methodology to temporally interpolate sparse snapshot estimates of land surface variables into daily time steps relying on UAS observations. Specific objectives were (1) to develop an operational 'top-down' model to simulate rapidly changed variables e.g. T_s, Rn, SM. ET and GPP to interpolate between remote sensing snapshot estimates; (2) to demonstrate the application of this model with UAS observations, calibrating the model with UAS

5   snapshot estimates and forcing with meteorological data and statistically interpolated VI.

2 Study site and data

2.1 Study site

This study was conducted in an eddy covariance flux site, Risoe (DK-RCW), which is an 11-hectare willow bioenergy plantation adjacent to the DTU Risoe campus, Zealand, Denmark (55.68°N, 12.11°E), as shown in Figure 1. This site has a

10   temperate maritime climate with mean annual temperature around 8.5°C and precipitation around 600 mm·yr^{-1}. The soil texture of this site is loam. The stand consists of two clones ('Inger' and 'Tordis') from crossing of *Salix viminalis*, *Salix schwerinii* x *Salix triandra*. In February of 2016, the aboveground parts were harvested following the regular management cycle. Then willow trees grew to a height of approximately 3.5m during the growing season of 2016 (May to October). Rapeseed (*Brassica napus*) was grown in the nearby field. A grass bypass is between the willow plantation and the rapeseed field. An eddy

15   covariance observation system (DK-RCW) has been operated since 2012. Regular UAS flight campaigns with a multispectral camera (MCA, Multispectral Camera Array, Tetracam, Chatsworth, CA, USA) and a thermal infrared camera (FLIR Tau2 324, Wilsonville, OR, USA) onboard have been conducted in this site during the growing seasons of 2016. Details refer to Wang et al. (2018b).
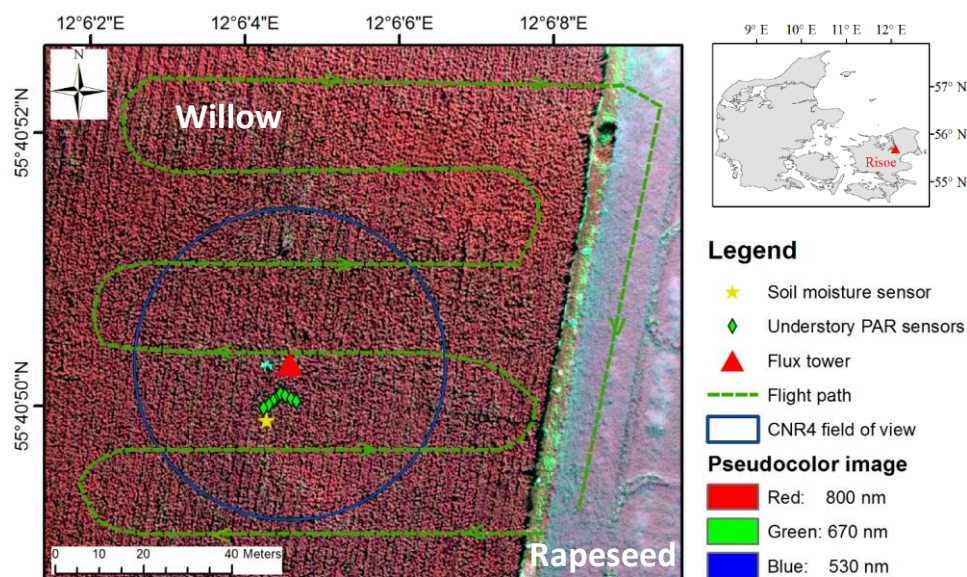
Figure 1. Overview of the Risoe willow plantation eddy covariance flux site. The flux tower is the red triangle in the middle of the willow plantation. The green dashed line shows the typical flying path of UAS. Green diamonds indicate the location of the understory PAR sensors. The yellow star is the location of soil moisture sensor. The blue circle indicates the CNR4 field of view. The base map is a multispectral pseudo-colour image with 800, 670 and 530 nm as red, green and blue channels.

2.2 Data

In-situ data used in this study include standard eddy covariance and micrometeorological observations, such as GPP, ET, Rn, incoming longwave radiation (LW_{in}), outgoing longwave radiation (LW_{out}) and incoming shortwave radiation (SW_{in}), air temperature (T_a), vapor pressure deficit (VPD) and SM. The eddy covariance data processing followed the same procedures as in Pilegaard et al. (2011), Ibrom et al. (2007) and Fratini et al. (2012), i.e. the standard ICOS processing method. The raw data were aggregated into half hourly records. The flux partitioning to separate GPP and respiration was done by the look-up table approach (Reichstein et al., 2005) based on the R-package REddyProc (Wutzler et al., 2018) with the half-hourly net ecosystem exchange, T_a and SW_{in} as inputs.

An UAS equipped with MCA and FLIR cameras was used to collect the Normalized Difference Vegetation Index (NDVI) and land surface temperature (T_s) (Wang et al., 2019). For each flight campaign, the digital surface model (DSM), multispectral reflectance and thermal infrared orthophotos were generated. For details on the UAS, sensors and image processing, refer to Wang et al. (2018b). To continuously estimate the land surface fluxes from UAS, the collected mean NDVI for the willow patch was temporally statistically interpolated into half-hour continuous records by the Catmull-Rom spline method (Catmull and Rom, 1974). The NDVI was converted into the fraction of intercepted photosynthetically active radiation (f_{IPAR}), which can also be assumed equal to the fraction of vegetation cover, based on Fisher et al. (2008). The canopy height h_c was obtained from the DSM generated from RGB images and then was statistically interpolated into the continuous half-hourly record based on in-situ f_{IPAR}. The collected T_s and NDVI from UAS were used to estimate the volumetric SM based on the modified temperature-vegetation triangle approach as Wang et al. (2018b). Values of the observed NDVI, T_s and the estimated SM from each UAS flight campaign are shown in Table 1. The statistically interpolated NDVI and h_c were used as model inputs/forcing.

Due to technical issues, data of few UAS flight campaigns were missing as shown in Table 1. The observed data from the in-situ measurements were used to represent these missing values. To fill a prolonged gap for UAS observations in June of 2016 and resemble the growth process of willow trees, a data point based on in-situ observations was added to June 24th. For model calibration, the instantaneous values of the T_s and SM estimated from the seven UAS flights were used as "ground truth" or observations. The seven UAS flights resulted in an average frequency of 25 days for this growing season. The minimum revisit time was 10 days between May 2nd and May 12th, which corresponded to the willow emerging period with a high growth rate. The maximum revisit time was 67 days between August 1st to October 7th when the willow canopy was dense and stable.
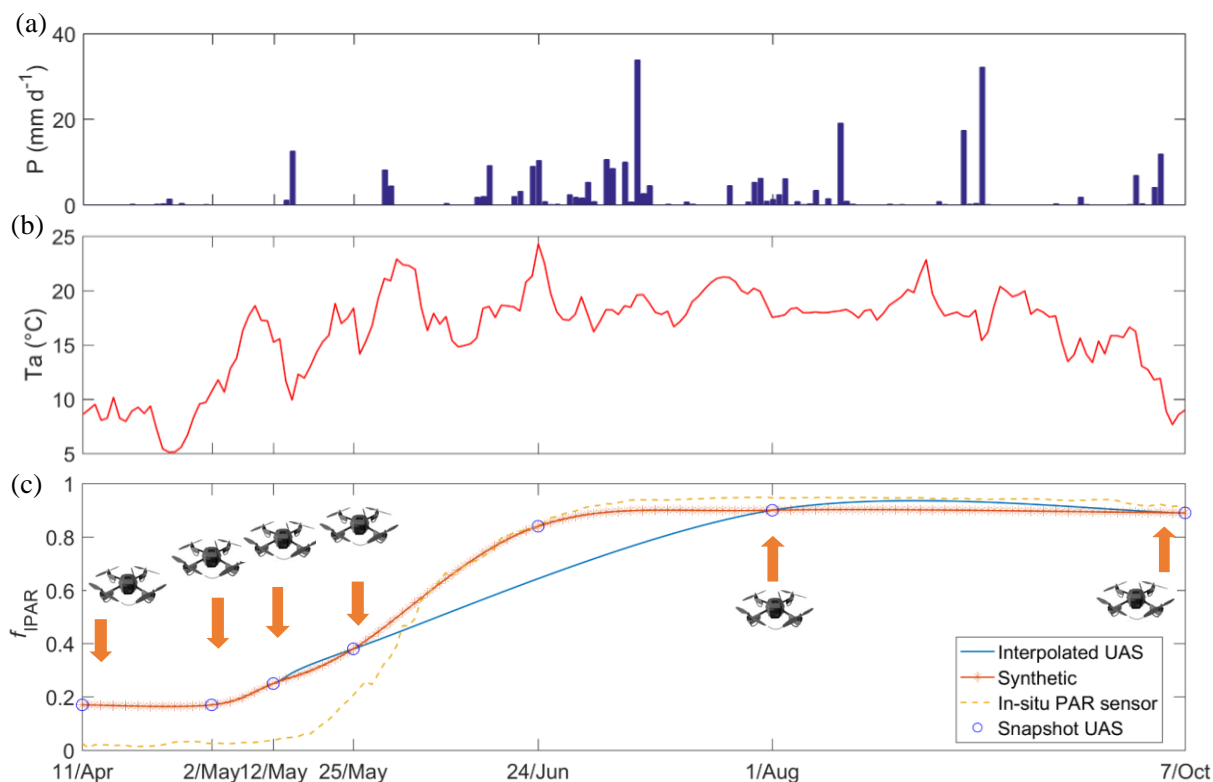
Figure 2. (a) Daily precipitation (P, mm·d^{-1}), (b) Daily air temperature (T$_a$, °C), and (c) Daily fraction of the intercepted PAR (f_{IPAR}) interpolated from UAS based NDVI during the growing season of 2016.

5   **Table 1**. NDVI, LST and SM information from UAS and in-situ data. * indicates that no available data from UAS due to technical issues and the in-situ data were used to represent the UAS snapshots. f_{IPAR} is the fraction of the intercepted PAR. T$_s$ is the land surface temperature (°C). θ is the volumetric SM (m^3·m^{-3}). For methods on SM estimation and detailed weather conditions, please refer to Wang et al. (2018b).

Date	Acquisition time	Weather	f_{IPAR} UAS	f_{IPAR} obs	T$_s$ UAS	T$_s$ obs	θ UAS	θ obs	Growth stage
11-Apr-16	11:13-11:26	Cloudy	0.22	0.03	14.98	15.95	0.27	0.28	Early growth
2-May-16	14:40-14:55	Cloudy	0.22	0.03	18.29	19.13	0.27	0.30	Early growth
12-May-16	10:44-11:55	Sunny	0.3	0.04	24.84	23.57	0.25	0.27	Early growth
25-May-16	10:11-10:23	Sunny	0.43	0.20	28.08	28.31	0.26	0.26	Early growth
24-Jun-16	12:00-12:30	Sunny	0.84*	0.84	26.60*	26.60	0.21*	0.21	Dense vegetation
1-Aug-16	10:06-10:14	Cloudy	0.95	0.95	18.33*	18.33	0.20*	0.20	Dense vegetation
7-Oct-16	11:41-11:55	Sunny	0.94	0.91	11.10	10.41	0.16	0.19	Dense vegetation

3 Method

The SVEN model is an operational and parsimonious remote sensing based land surface modeling scheme expanding the capabilities of the remote sensing GPP and PT JPL-ET model (Wang et al., 2018a) to be dynamic. It runs at half-hourly time steps and can facilitates to temporally interpolate the simulated instantaneous land surface variables, such as T_s, Rn, SM, ET

5 and GPP into continuous records.

3.1 Model description

SVEN consists of a surface energy balance module, a water balance module and a CO_2 flux module. In the energy balance module, SVEN estimates the surface temperature and ground heat flux relying on the land surface energy balance equations and the 'force-restore' method (Noilhan and Mahfouf, 1996; Noilhan and Planton, 1989). The water balance module includes

10 the Priestley–Taylor Jet Propulsion Laboratory (PT-JPL) model for ET estimation and a simple 'bucket' model representing the upper soil column to simulate soil water dynamics and runoff generation. The CO_2 flux module uses a light use efficiency (LUE) model for GPP estimation, which is connected to ET via the same canopy biophysical constraints. Figure 3 shows the major processes simulated in SVEN. Detailed information on these three modules is outlined below.
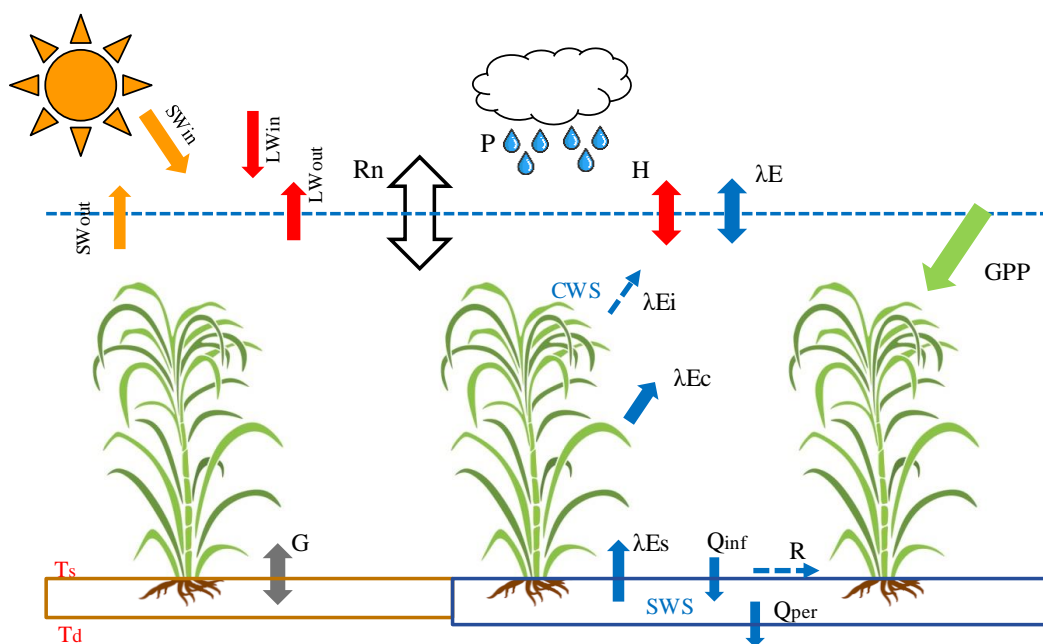
15 **Figure 3**. Major land surface processes simulated in SVEN. These processes include land surface energy balance, water fluxes and CO_2 assimilation (SW$_{in}$: incoming shortwave radiation; SW$_{out}$: outgoing shortwave radiation; LW$_{in}$: incoming longwave radiation; LW$_{out}$: outgoing longwave radiation; Rn: net radiation; G: ground heat flux; T_s: the surface temperature; T_d: the deep soil temperature; H: sensible heat flux; P: precipitation; λE: latent heat flux; λEi: latent heat flux of the intercepted water; λEc:

latent heat flux of transpiration; λEs: latent heat flux of soil evaporation; CWS: canopy water storage; SWS: soil water storage; Q_{inf}: infiltration; Q_{per}: percolation; R: surface runoff; GPP: gross primary productivity.

3.1.1 Surface Energy Balance Module

The instantaneous net radiation is estimated based on the surface energy balance, as shown in Eq. (1). The surface emissivity is approximated according to an empirical relation with NDVI as Eq. (2) (Van de Griend and M.Owe., 1993). The surface albedo (ALB) is estimated from the simple ratio vegetation index (SR) and it shows that albedo generally decreases as vegetation greenness increases as Eq. (3 and 4) (Gao, 1995).

$$Rn = (1 - ALB)SW_{in} + (1 - \varepsilon)LW_{in} - \varepsilon\sigma T_s^4 \tag{1}$$

$$\varepsilon = \begin{cases} 0.986 & (NDVI > 0.608) \\ 1.0094 + 0.047 \cdot \ln(NDVI) & (0.131 < NDVI < 0.608) \\ 0.914 & (NDVI < 0.131) \end{cases} \tag{2}$$

$$ALB = 0.28 - 0.14e^{(-6.08/SR^2)} \tag{3}$$

$$SR = (1 + NDVI)/(1 - NDVI) \tag{4}$$

Where Rn is the instantaneous net radiation (W·m^{-2}). SW_{in} is the instantaneous incoming shortwave radiation (W·m^{-2}). LW_{in} is the instantaneous incoming longwave radiation (W·m^{-2}). σ is the Stefan-Boltzmann constant (5.670367×10^{-8} W·m^{-2}·K^{-4}).

At the surface, Rn is dissipated as latent, sensible and ground heat fluxes, as Eq. (5). The latent heat flux is estimated from the PT-JPL ET model and the sensible heat flux, H, is calculated based on the temperature gradient between the surface and air and a bulk aerodynamic resistance. The instantaneous ground heat flux G is estimated from the ´force-restore´ method (Noilhan and Planton, 1989).

$$\frac{dS}{dt} = SW_{in} - SW_{out} + LW_{in} - LW_{out} - H - \lambda E - G \tag{5}$$

Where $\frac{dS}{dt}$ is the heat storage change over time (W·m^{-2}). SW is shortwave radiation (W·m^{-2}) and LW is longwave radiation (W·m^{-2}). The subscripts $_{in}$ and $_{out}$ refer to incoming and outgoing, respectively. λE represents the latent heat flux (W·m^{-2}). H refers to the sensible heat flux (W·m^{-2}). G is the ground heat flux (W·m^{-2}).

The surface temperature was estimated by the 'force-restore' method, which considers two opposite effects on surface temperature variabilities, as shown in Eq. (6). The first term $(R_n - \lambda E - H)$ represents the forcing from the surface-atmosphere interface. The second term $(T_s - T_d)$ is the gradient between the surface temperature and deep soil temperature. It indicates the tendency from the deep soil to restore T_s (responding to surface energy forcing) to the T_d value, which is more stable over time.

$$\frac{dT_s}{dt} = C_T(R_n - \lambda E - H) - C_d(T_s - T_d) \tag{6}$$

$$\frac{dT_d}{dt} = \omega(T_s - T_d) \tag{7}$$

$$\frac{1}{C_T} = \frac{1-f_c}{C_{sat}(\frac{SWS_{max}}{SWS})^{\frac{b}{2\ln(10)}}} + \frac{f_c}{C_{veg}} \tag{8}$$

$$C_d = 2\pi\omega \tag{9}$$

Where T_s is the land surface temperature (°C). T_d is the deep soil temperature (°C) calculated by applying a low-pass filter to T_s. ω is the frequency of oscillation 1/24 (h^{-1}). C_T is a force-restore thermal coefficient for the surface heat transfer (K·m^2·J^{-1}) and is influenced by the effective relative SM. C_{sat} is the force-restore thermal coefficient for saturated soil (K·m^2·J^{-1}). The parameter b is the slope of the retention curve for the force-restore thermal coefficient. C_{veg} is the force-restore thermal coefficient for vegetation (K·m^2·J^{-1}). f_c is the fractional cover of vegetation and is assumed equal to f_{IPAR} as the supplemental Table S1 (Fisher et al., 2008). SWS$_{max}$ is the maximum soil water storage (m^3) and SWS is the actual one (m^3). C_d is diurnal periodicity based on ω (h^{-1}).

The sensible heat flux, H, is estimated based on the temperature gradient between the surface and air, as shown in Eq. (10).

$$H = \rho c_p(T_s - T_a)/r_a \tag{10}$$

Where ρ is the air density (kg·m^{-3}). c_p is the specific heat capacity of air (J·kg^{-1}·K^{-1}). T_s is the land surface temperature (°C). T_a is the air temperature (°C). r_a is the aerodynamic resistance for heat transfer (s·m^{-1}).

Aerodynamic resistance to turbulent transport under neutral conditions (r_{aN}) can be expressed as Eq. (11) (Brutsaert, 1982).

$$r_{aN} = \frac{\ln\left(\frac{z-d}{z_{om}}\right)\ln\left(\frac{z-d}{z_{oh}}\right)}{k^2 u} \tag{11}$$

$$d = 0.67h_c \tag{12}$$

$$z_{om} = 0.1h_c \tag{13}$$

$$z_{oh} = \frac{z_{om}}{e^{kB^{-1}}} \tag{14}$$

Where h_c is the canopy height (m). The parameter d is the zero displacement height (m) and z is the velocity reference height (m). z_{om} is the aerodynamic roughness length for momentum (m). z_{oh} is the aerodynamic roughness length for the heat transfer (m). u is the horizontal wind velocity at reference height (m·s^{-1}). kB^{-1} is a parameter to account for the difference between the aerodynamic and radiometric temperatures and a constant value of 2.3 is adopted in this study (Garratt and Hicks, 1973). k is von Karman constant (0.4).

The aerodynamic resistance is corrected for the atmospheric stability as shown in Eq. (15) (Huning and Margulis, 2015). Ψ_m is the stability correction factor for momentum. Ψ_h is the stability correction factor for sensible heat flux. For unstable conditions (negative temperature gradient), the stability correction factors are less than 1.0 and the correction reduces the resistance and enhances turbulence, while for stable conditions they are greater than 1.0 and the correction increases the resistance and suppresses turbulence.

$$r_a = r_{aN} \Psi_m \Psi_h \tag{15}$$

When atmospheric condition is unstable ($R_{iB} \leq 0$), Ψ_m and Ψ_h are estimated from Eq. (16).

$$\Psi_h = {\Psi_m}^2 = (1 - 15R_{iB})^{-1/2} \tag{16}$$

When atmospheric condition is stable ($0 \leq R_{iB} < 0.2$), Ψ_m and Ψ_h are estimated from Eq. (17).

$$\Psi_h = \Psi_m = (1 - 5R_{iB})^{-1} \tag{17}$$

$$R_{iB} = \frac{\left(\frac{g}{Ts}\right) \partial Ts/\partial z}{(\frac{\partial u}{\partial z})^2} \tag{18}$$

Where R_{iB} is the bulk Richardson number, g is the gravitational acceleration.

3.1.2 Water balance module

The water balance module simulates evaporation of intercepted water, plant transpiration, soil evaporation, soil infiltration and percolation. The evapotranspiration is estimated based on a modified PT-JPL ET model (Wang et al., 2018a). The PT-JPL ET model has been demonstrated as one of best-performing global remote sensing ET algorithms (Chen et al., 2014; Ershadi et al., 2014; Miralles et al., 2016; Vinukollu et al., 2011). Thus, it was selected for ET estimation. The PT-JPL model (Fisher et al., 2008) uses the Priestley-Taylor (1972) equation to calculate the potential evapotranspiration, and then incorporates eco-physiological variables to down regulate potential evapotranspiration to actual evapotranspiration. PT-JPL is a three-source evapotranspiration model to simulate evaporation of intercepted water (Ei), transpiration (Ec) and soil evaporation (Es) as following equations.

$$\lambda ET = \lambda Ei + \lambda Ec + \lambda Es \tag{19}$$

$$\lambda Ei = f_{wet} \cdot \alpha \Delta / (\Delta + \gamma) \cdot Rnc \tag{20}$$

$$\lambda Ec = (1 - f_{wet}) \cdot f_g \cdot f_M \cdot f_{Ta} \cdot \alpha_c \Delta / (\Delta + \gamma) \cdot Rnc \tag{21}$$

$$\lambda Es = f_{SM} \cdot \alpha \Delta / (\Delta + \gamma) \cdot (Rns - G) \tag{22}$$

Where λET is the latent heat flux for total evapotranspiration (W·m⁻²), λEi is the latent heat flux due to evaporation of intercepted water (W·m⁻²), λEc is the latent heat flux due to transpiration (W·m⁻²), and λEs is the latent heat flux due to

evaporation of soil water (W·m⁻²). The quantity f_{wet} is the relative surface wetness to partition the evapotranspiration from the intercepted water and canopy transpiration. f_g is the green canopy fraction indicating the proportion of active canopy. f_M is the plant moisture constraint. f_{Ta} is the plant temperature constraint reflecting the temperature limitation of photosynthesis. f_{SM} is the SM constraint. These constraints vary from 0 to 1 to account for the relative reduction of potential λET under limiting

5 environmental conditions. Rnc and Rns are the net radiation for canopy and soil, respectively. The partitioning of PAR and net radiation between canopy and soil is calculated following the Beer-Lambert law (Supplemental Table S1). G is the ground heat flux. Δ is the slope of saturation vapor pressure versus temperature curve. γ is the psychrometric constant. α is an empirical ratio of potential evapotranspiration to equilibrium potential evapotranspiration (PT coefficient). The suggested value for α is 1.26 in the PT-JPL model (Fisher et al., 2008).

10 In the original model, f_{wet} was estimated from air relative humidity (Fisher et al., 2008). In this study, f_{wet} is modified to be defined as a ratio between the actual canopy water storage (CWS) and the maximum canopy water storage (CWS$_{max}$) as Eq. (23) (Noilhan and Planton, 1989). CWS is the amount of intercepted water and CWS$_{max}$ is the maximum possible amount of intercepted water (mm), taken as 0.2LAI kg·m⁻² (Dickinson, 1984). f_{wet} depends on both the precipitation rate and LAI, which is more reasonable than only depending on air relative humidity in the original model.

15 $$f_{wet} = \frac{CWS}{CWS_{max}} \tag{23}$$

In this study, we determined CWS with a prognostic equation (24) with the constraint that CWS is smaller than CWS$_{max}$.

$$\frac{dCWS}{dt} = f_c \cdot P - Ei \tag{24}$$

Where f_c is the fraction of vegetation cover and here it is assumed to be equal to f_{IPAR} (Fisher et al., 2008). P and Ei are the rainfall rates and evaporation from the intercepted water, respectively (m·s⁻¹).

20 The effective precipitation rate is estimated as the residual of the rainfall rate and change of CWS as Eq. (25).

$$P_e = P - dCWS \tag{25}$$

To simulate the dynamics of water storage in the soil, SVEN uses a simple 'bucket' model. Here the infiltration rate (Q$_{inf}$) is equal to the effective rainfall rate (P$_e$), when the soil water is not saturated. Thus, SWS is calculated based on a prognostic equation with a constraint that SWS is smaller than SWS$_{max}$.

25 $$Q_{inf} = P_e \tag{26}$$

$$\frac{dSWS}{dt} = Q_{inf} - Ec - Es - Q_{per} \tag{27}$$

When soil water is saturated, SWS is equal to SWS$_{max}$ and surface runoff (R) occurs as Eq. 28.

$$Q_{inf} = Ec + Es + Q_{per} \tag{28}$$

$$R = P_e - Q_{inf} \tag{29}$$

Where SWS is soil water storage (m). P_e, E_c, E_s, Q_{per} and R are the effective rainfall rates, transpiration rates, evapotranspiration rates from soil, percolation rates and surface runoff (m·s⁻¹), respectively.

Percolation is estimated by assuming uniform vertical hydraulic gradient and using the Mualem model for hydraulic
5   conductivity of unsaturated soils (Mualem, 1976) as Eq. (30):

$$Q_{per} = K_s\sqrt{\theta_e}(1 - (1 - \theta_e^{1/(1-1/n)})^{1-1/n})^2 \tag{30}$$

$$\theta_e = \frac{\theta - \theta_r}{\theta_s - \theta_r} \tag{31}$$

$$\theta = \frac{SWS}{SWS_{max}}\theta_s \tag{32}$$

Where K_s is the saturated hydraulic conductivity (m·s⁻¹). n is a fitting parameter depending on the pore size. θ is the volumetric
10   soil moisture (m³·m⁻³). θ_e is the effective soil moisture (m³·m⁻³). θ_s is the saturated soil moisture (m³·m⁻³). θ_r is the residual soil moisture (m³·m⁻³).

3.1.3 CO₂ flux module

The photosynthesis in the CO₂ flux module is calculated from a modified light use efficiency (LUE) model (Wang et al., 2018a) linked to the biophysical constraints for canopy transpiration of the PT-JPL model. The LUE GPP model is a robust
15   and widely used method to estimate GPP across various ecosystems and climate regimes (McCallum et al., 2009). The LUE models e.g. CASA (Potter et al., 1993) or the MODIS algorithm (Running et al., 2004) are based on the assumption that plants optimize canopy LUE or whole canopy carbon gain per total PAR absorbed as originally suggested by (Monteith, 1972) for net primary productivity. The formula of the LUE GPP model used in this study is shown in Eq. (33) and it is partly based on the Carnegie-Ames-Stanford-Approach model (Potter et al., 1993) with modification to include an additional constraint
20   accounting for the fraction of the canopy that is photosynthetically active (Fisher et al., 2008). The rest of constraints reflects changes in LUE due to environmental factors such as thermal regulation (Wang et al., 2018a) and are the same modifying the ETc (Eq. 21).

$$GPP = LUE_{max} \cdot PARc \cdot f_g \cdot f_M \cdot f_{Ta} \cdot f_{VPD} \tag{33}$$

Where LUE_{max} is the maximum LUE (g·C·MJ⁻¹). PARc is the daily photosynthetically active radiation (PAR) (MJ·m⁻²·d⁻¹)
25   intercepted by the canopy and it is calculated based on the extinction of PAR within the canopy using the Beer Lambert law (Supplemental Table S1). f_g is the green canopy fraction indicating the proportion of active canopy. f_M is the plant moisture constraint. f_{Ta} is the air temperature constraint reflecting the temperature limitation of photosynthesis. f_{VPD} is the VPD constraint reflecting the stomatal response to the atmospheric water saturation deficit. All these constraints range from 0 and

1 and represent the reduction of maximum GPP under limiting environmental conditions. For more details, please refer to the supplemental Table S1.

3.2 Model parameter estimation

The SVEN model requires shortwave incoming (SW_{in}), longwave incoming (LW_{in}), air temperature (T_a), air pressure (P_s),

5 relative humidity (RH), wind speed (WS), precipitation (P), canopy height (z), and vegetation information (NDVI) as inputs (Supplemental Table S2). The model inputs of this study were obtained from meteorological data and UAS observations. The simulation outputs of this model are shown in Supplemental Table S4. The initial conditions for the model include an initial canopy water storage (CWS_{in}), an initial soil water storage (SWS_{in}), initial surface temperature (T_{s0}) and initial deep soil temperature (T_{d0}) as shown in Supplemental Table S3. The initial conditions to run the model (11-April-2016 to 7-October-

10 2016) were obtained by performing spin-up simulations from 11-March-2016 to 11-April-2016.

The SVEN model has six parameters, which are mostly related to physical soil properties for heat transfer and infiltration (Table 2). The parameter values can be obtained from several approaches including look-up tables based on soil texture, parameter values of the similar biome or soil types in other studies, field measurements, or model parameter optimization with in-situ measurements or with remote sensing data. The parameters, for instance maximum light use efficiency (LUE_{max}), to

15 run the snapshot version of SVEN are described in Wang et al., (2018a). As this willow plantation is a deciduous temperate forest, the parameter values obtained from the nearby similar ecosystem (Wang et al., 2018a) were used for this study.

Table 2. Information on the model parameters of SVEN and their ranges for all soil or biome types

Parameters	Description	Unit	Range	Reference
C_{sat}	The force-restore thermal coefficient for saturated soil	10^{-6} K·m²·J^{-1}	[3, 15]	Noilhan and Planton (1989)
b	The slope of the retention curve for the force-restore thermal coefficient	[-]	[4.05, 11.4]	Noilhan and Planton (1989)
C_{veg}	The force-restore thermal coefficient for vegetated surface	10^{-6} K·m²·J^{-1}	[1, 10]	Calvet et al. (1998)
SWS_{max}	Maximum soil water storage	m	[0, 1]	Boegh et al. (2009)
K_s	The infiltration rate for the saturated soil	mm·h^{-1}	[0.01, 25]	Dettmann et al. (2014)
n	Fitting parameter of the Mualem model	\	[1, 3]	Dettmann et al. (2014)

In this study, we used a combination of these approaches to obtain model parameter values. The fitting parameter of the

20 Mualem model (n) and the infiltration rate for the saturated soil (K_s) were obtained from a look-up table (Carsel and Parrish, 1988). The values for loamy soil as shown in the supplemental Table S5 were used, according to the soil texture of this site. The rest of parameters related with soil and vegetation physical properties, C_{sat}, b, C_{veg} and SWS_{max}, were obtained by calibrating models with instantaneous T_s and SM from seven UAS flight campaigns (Table 1) rather than calibration with in-situ measurements of ET or GPP (e.g. eddy covariance data) as in other studies. Calibrating the model with the remotely sensed

instantaneous estimates instead of ground measurements facilitate the application of this approach to data scarce regions. The calibration of C_{sat}, b, C_{veg} and SWS_{max} was conducted using the Monte Carlo optimization. The parameter values were sampled 20,000 times with a uniform distribution and corresponding parameter ranges as shown in Table 2. The objective function for optimization is the root mean square deviation (RMSD) between the observed and simulated values. With two objective

5   functions for T_s and SM respectively, a multiple objective optimization method (Pareto front) as Yapo et al. (1998) was used to identify the optimized parameter values.

3.3 Model assessment

We used independent eddy covariance data to validate model outputs. However, due to the energy balance closure issue (Wilson et al., 2002), the sum of sensible heat (H) and latent heat (LE) as measured by the eddy covariance method is generally

10   not equal to the available energy (net radiation minus ground heat flux, $R_n - G$). This study used the Bowen ratio approach to correct energy balance closure errors of eddy covariance data. Assuming that the ratio of sensible heat to ET (Bowen ratio) is correct, LE measurements can be corrected as follows (Twine et al., 2000). The LE data with the energy balance closure error larger than 20% were excluded in the validation.

$$LE = \frac{R_n - G}{H\_EC\_raw + LE\_EC\_raw} LE\_EC\_raw \qquad (34)$$

15   Where LE is the corrected latent heat by assuming that the Bowen ratio is constant (W·m⁻²). R_n is the net radiation (W·m⁻²). G is the ground heat flux (W·m⁻²). H_EC_raw is the uncorrected sensible heat (W·m⁻²) and LE_EC_raw is the uncorrected latent heat (W·m⁻²).

The SVEN model was developed to interpolate between remote sensing data acquisitions and to produce continuous daily records. Thus, the observed T_s, Rn, LE and GPP are from the eddy covariance system and the in-situ SM measurements at the

20   depth of 15 cm (the sensor locations shown in Figure 1) were used to validate the simulated variables at the daily time scale. Statistics including RMSD, correlation coefficient (R) and relative errors (RE) were used in validation.

We also analyzed how the model skill changes depending on vegetation cover and overcast (diffuse radiation) conditions by looking at model residuals as typically remote sensing models may be biased to sunny conditions. Scatterplots between model residuals and NDVI and the diffuse radiation fraction were examined. As the ratio between the actual (SW_{in}) and potential

25   ($SW_{in}pot$) can well represent the diffuse radiation fraction (Wang et al., 2018a), we used this ratio to indicate the diffuse radiation fraction. This analysis can help to understand possible methods to improve the SVEN model. To check the capability of the SVEN model to interpolate half-hourly and monthly time series fluxes, the simulated land surface variables were also validated at half-hourly and monthly time scales, in addition to the daily time scale.

4 Results and discussion

4.1 Model parameter estimation

Figure 4 illustrates the results of model parameter calibration with UAS based snapshot SM and T_s (Table 1). With two objective functions, RMSDs of SM and T_s, a significant trade-off between the performance of the SM and T_s simulations is

5   observed as a Pareto front (the red curve) in Figure 4. The x-axis shows the performance of simulating SM. The smaller the RMSD values are, the better the model performance with respect to this variable. The minimum, however, lies in a range, where the model performance of the other variable, T_s, is highest (y-axis). From the viewpoint of multi-objective optimization, the solutions at the Pareto front are equally good. By considering RMSDs of T_s less than 2 °C and RMSDs of SM estimates as small as possible, we selected the point close to the red arrow of Figure 4, which corresponds to the RMSDs of SM and T_s

10   equal to 2.99% $m^3 \cdot m^{-3}$ and 1.92 °C, respectively. The values of C_{sat}, b, C_{veg} and SWS_{max} at this Pareto front point are equal to 6.94×10^{-6} $K \cdot m^2 \cdot J^{-1}$, 5.20, 2.18×10^{-6} $K \cdot m^2 \cdot J^{-1}$ and 554.52 mm, respectively.
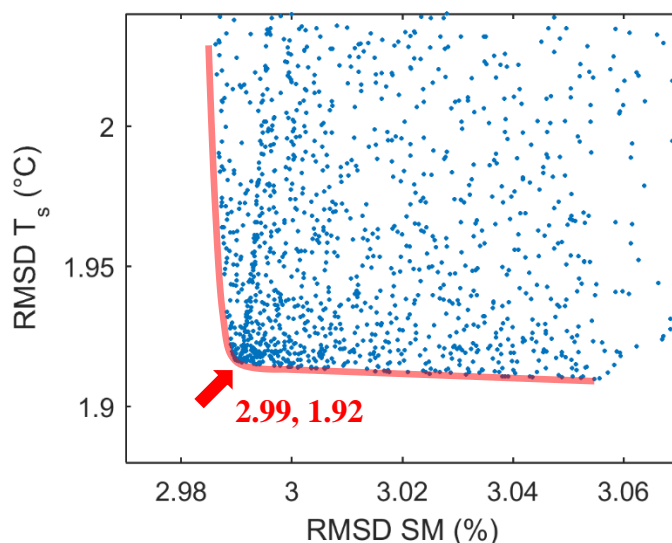
Figure 4. Objective function values of evaluated parameter sets and corresponding Pareto front. The x-axis is the objective function for simulating SM. The y-axis is the objective function for simulating T_s. Each dot corresponds to one simulation

15   performance. Each of the simulations represents a different combination of candidate parameter sets. The dot closest to the red arrow is chosen to be the optimal parameter set for SVEN continuous simulation.

4.2 Validation at the daily time scale

Figure 5 shows the time series data of the interpolated daily T_s, Rn, SM, LE and GPP and their validation. It can be seen that the simulated daily T_s, Rn, SM, LE and GPP fits well with observations at this site. RMSDs for the simulated daily T_s, Rn,

20   SM, LE and GPP are 2.35 °C, 14.49 $W \cdot m^{-2}$, 1.98% $m^3 \cdot m^{-3}$, 16.62 $W \cdot m^{-2}$ and 3.01 $g \cdot C \cdot m^{-2} \cdot d^{-1}$, respectively. R^2 for T_s, Rn, SM,

LE and GPP are 0.90, 0.92, 0.50, 0.70 and 0.79, respectively. RE for T_s, Rn, SM, LE and GPP are 10.47%, -2.96%, -1.05%, 9.23% and -14.53%, respectively. This demonstrates that SVEN is capable to temporally interpolate between the remote sensing data acquisitions and interpolate the snapshot estimates or observations to form continuous daily records.

For the simulated T_s, it can be seen that during the early growth stage (before June), the SVEN model simulated quite accurately

5   the temporal dynamics. However, during the dense vegetation stage (high NDVI), the model tends to overestimate T_s. Similarly, for Rn, during the early growth stage, the model underestimated Rn, while it overestimated Rn for the dense vegetation stage. These biases can also be identified from the scatterplots between model residuals and NDVI. As shown in Figure 6 (a-b), with low NDVI, the model underestimates Rn and vice-versa. With high NDVI the simulated T_s shows overestimation. One of reasons for this error could be the uncertainty in the estimated surface albedo. The albedo in the SVEN

10   model was determined by the simple empirical formula as Eq. (3) with a high value in the early growth stage and a low value for dense vegetation. Another possible source for errors is from uncertainties in C_{veg}, which reflects the thermal storage property of vegetated surface in the force-restore method. C_{veg} was obtained from model calibration with UAS T_s. As shown in Figure 1, only three UAS data sets were available in the vegetated period. The insufficient model calibration may lead to the uncertainties in C_{veg}.

15   Figure 5 (c) shows that the estimated SM from the SVEN model achieved a moderate performance in terms of error and correlation. The model underestimates SM when NDVI is low, and overestimates SM when NDVI is high as shown in Figure 6 (c). This may be due to the uncertainty in the model parameters related to SM and the error propagation from the remote sensing based SM. As shown in supplemental Table S5, the effective parameter values of the infiltration rate for the saturated soil (Ks) and fitting parameter of the Mualem model (n) were taken as the mean values from the look-up table without

20   considering ranges of variability (standard deviations in the table). In fact, only one parameter, SWS_{max}, among the three parameters related to SM dynamics was calibrated with UAS estimates of SM in the root zone. Additionally, the SM estimates used for calibration have also errors of around 13% (Wang et al., 2018a) that can propagate in the parameter calibration. Furthermore, only seven snapshot estimates from UAS were used to calibrate the model with an average frequency of 25 days during the period of fast growth. It can be expected that the better UAS based snapshot estimates of SM and increasing the

25   number of observations for model calibration can improve the simulation performance.

The results of the simulated LE and GPP are shown in Figure 5 (d) and (e), respectively. It can be seen that the simulation overestimated LE. This can be improved with better estimates of Rn and SM. From the scatterplot of Figure 5 (e), the simulation underestimated GPP, as the parameter LUE_{max} was assumed to be the same as from a nearly beech forest (Wang et al., 2018a). Even though both sites are temperate deciduous forests, there is difference between the natural beech forest and

30   the willow forest bioenergy plantation. It should be noted that there is a significant underestimation of the simulated GPP in June of 2016 as shown in Figure 5 (e). Besides the possible uncertainties from the LUE_{max} described above, this underestimation may also result from the partitioning of GPP and respiration in the eddy covariance data processing used in validation. In the data processing, the night time net ecosystem exchanges were used to calculate the ecosystem respiration. During the night time, the eddy covariance footprint has a large coverage due to the stable atmospheric conditions. The

ploughing activities in the nearby field released CO_2 to the atmosphere. This could contribute overestimation of daytime ecosystem respiration and thus also leads to the overestimation of GPP in the eddy covariance data processing.
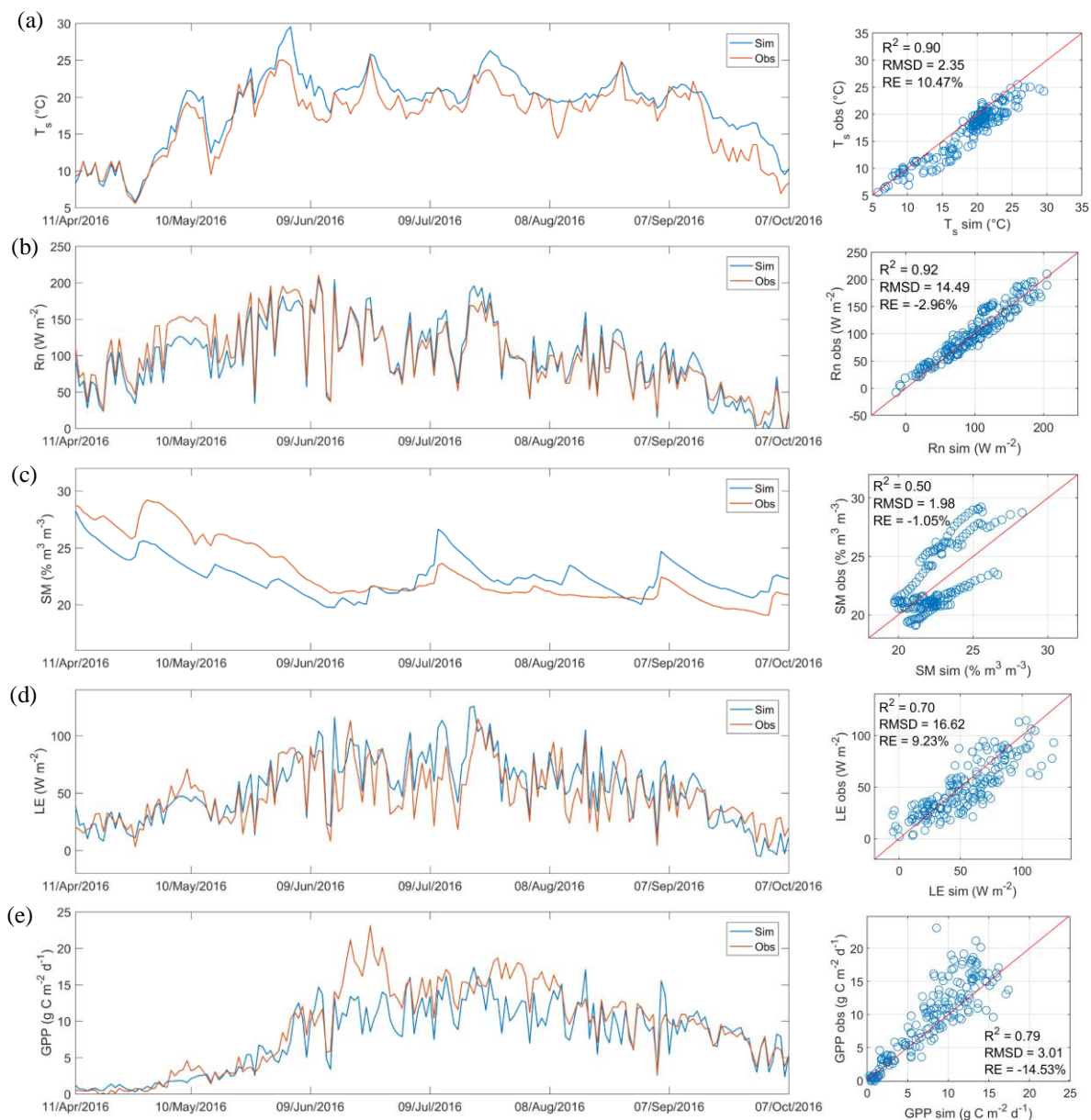
Figure 5. Simulated continuous daily land surface variables from 11th April to 7th October 2016 in the willow plantation. (a) Land surface temperature T_s, (b) Net radiation Rn, (c) Soil moisture SM, (d) Latent heat flux LE, and (e) Gross primary productivity GPP.

To check whether the model simulations are be good under overcast conditions, we analysed the relationship between model residuals and the ratio representing the diffuse radiation fraction and NDVI (Figure 6). Residuals of the simulated T_s, Rn, SM and LE do not show difference between low and high diffuse radiation fraction. The SVEN model was capable of interpolating LE and SM under cloud cover conditions with similar skill as under clear sky conditions but not GPP. GPP was underestimated under high diffuse radiation conditions and overestimated in the low diffuse radiation conditions. This is due to that the model did not consider the enhancement diffuse radiation effects on the plant carbon assimilation rate (Mercado et al., 2009; Roderick et al., 2001). It could be improved by incorporating an index representing the diffuse radiation fraction as Wang et al. (2018a), if higher accuracy is needed.
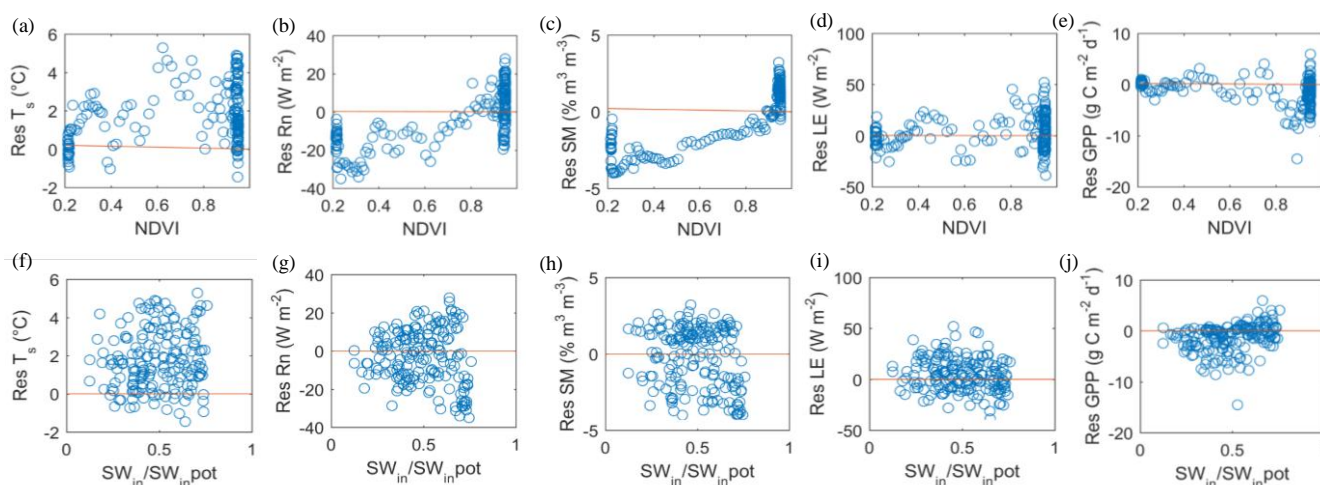
Figure 6. Model residuals for the daily simulation. (a-e) are relationship between model residuals and the ratio of the actual (SW_{in}) and potential ($SW_{in}pot$), which is an indicator for the diffuse radiation fraction. (f-j) are relationship between model residuals and NDVI. (a, f) surface temperature T_s, (b, g) net radiation Rn, (c, h) soil moisture SM, (d, i) latent heat flux LE, and (e, j) gross primary productivity GPP.

4.3 Validation at half-hourly and monthly time scales

Validation of the half-hourly and monthly T_s, Rn, SM, LE and GPP by the SVEN model is shown in Figure 7. The simulated half-hourly T_s, Rn, SM, LE and GPP captured the temporal dynamics of land surface fluxes at this site. RMSDs for T_s, Rn, SM, LE and GPP are 3.04 °C, 63.82 W·m⁻², 1.99% m³·m⁻³, 56.37 W·m⁻² and 6.14 μmol·C·m⁻²·s⁻¹, respectively. R^2 for T_s, Rn, SM, LE and GPP are 0.83, 0.89, 0.49, 0.78 and 0.77, respectively. At the monthly time scale, RMSDs for T_s, Rn, SM, LE and GPP are 2.10 °C, 10.96 W·m⁻², 1.86% m³·m⁻³, 9.09 W·m⁻² and 1.82 g·C·m⁻²·d⁻¹, respectively. R^2 for T_s, Rn, SM, LE and GPP are 0.96, 0.94, 0.61, 0.97 and 0.97, respectively. The metrics of RE for hourly and monthly scales are not shown, as they are the same as the RE at the daily scale. Compared to the simulation performance at the daily time scale (as shown in Table 3), the half-hourly simulation has higher RMSDs and lower R^2. However, the monthly simulation has better performance than the

daily with lower RMSDs and slightly higher R^2. When performing temporal averages, random errors cancel out. Additionally, the LE in SVEN model is based on the Priestley-Taylor equation originally applied to estimate monthly LE (Fisher et al., 2008) and was expended to be applied at daily steps (Garcia et al., 2013), but it is not appropriate for representing LE processes at sub-daily time scales. The improvement of model performance from the half-hourly to daily and monthly time scales indicates

5   the model errors can be reduced by aggregating the simulation outputs to longer time scales. This also implies that the SVEN model has greater potential to temporally interpolate remote sensing observations at daily and monthly time scales, which are more relevant for applications in agriculture and ecosystem management.
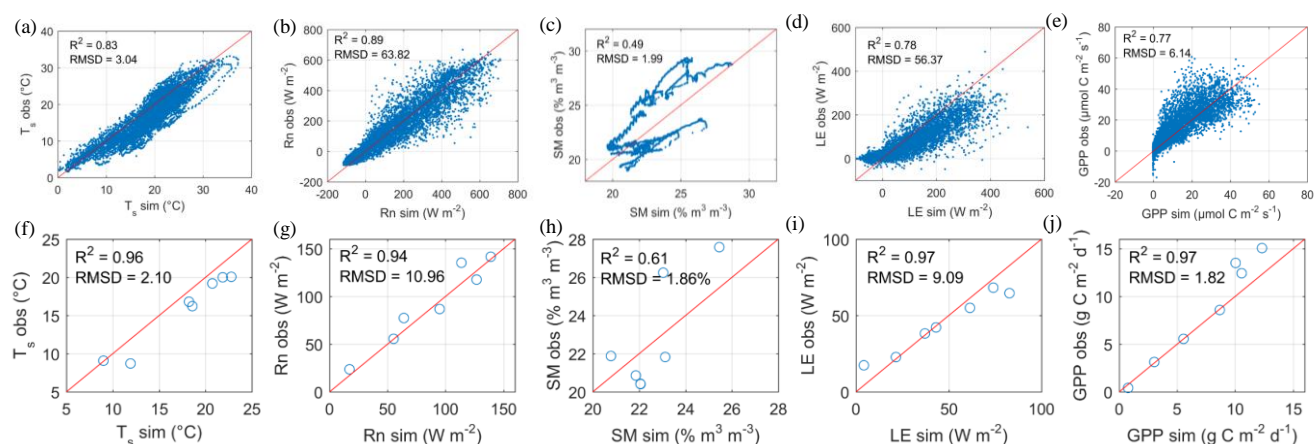
Figure 7. Validation of the gap filled land surface variables at half-hourly and monthly time scales in the willow plantation.
10   (a-e) are at half hourly time scale and (f-j) are at the monthly time scale. (a, f) land surface temperature T_s, (b, g) net radiation R_n, (c, h) soil moisture SM, (d, i) latent heat flux LE, and (e, j) gross primary productivity GPP.

Table 3. Comparison of model simulation performance at half hourly, daily and monthly time scales.

Time scale	Statistics	Ts	Rn	SM	LE	GPP
Half hourly	R^2	0.83	0.89	0.49	0.78	0.77
	RMSD	3.04 °C	63.82 W·m^{-2}	1.99% m^3·m^{-3}	56.37 W·m^{-2}	6.14 µmol·C·m^{-2}·s^{-1}
Daily	R^2	0.9	0.92	0.5	0.7	0.79
	RMSD	2.35 °C	14.49 W·m^{-2}	1.98% m^3·m^{-3}	16.62 W·m^{-2}	3.01 g·C·m^{-2}·d^{-1}
Monthly	R^2	0.96	0.94	0.61	0.97	0.97
	RMSD	2.1 °C	10.96 W·m^{-2}	1.86% m^3·m^{-3}	9.09 W·m^{-2}	1.82 g·C·m^{-2}·d^{-1}

4.4 Potential applications and improvement of SVEN model

This study showed that SVEN can be used as a tool to temporally interpolate land surface variables between remote sensing acquisitions with few meteorological data. In the statistical approaches, Alfieri et al. (2017) identified that a return interval of remote sensing observations should be no less than 5 days to accurately interpolate daily ET with relative errors less than 20%.

5 The results shown from our model based interpolation approach on a willow forest, suggests that the revisit time for the remote sensing observations can potentially be extended. For instance, this study demonstrated that seven instantaneous observations/simulations with an averaged revisit time of 25 days can be used to accurately interpolate the daily ET for 180 days. This shows the great benefits of using the model based approach to continuously estimate land surface fluxes from remote sensing based snapshot observations or simulations. The interpolated continuous record of land surface variables can further

10 facilitate our understanding on the temporal dynamics of land surface-atmosphere flux exchanges. On the other hand, this study also provides ideas to utilize remote sensing estimates or observations to improve land surface modeling. Traditionally, the applicability of land surface models is restricted due to complex model parameterization and the availability of "ground truth" or in-situ data for parameter calibration. As shown in this study, one solution for this is to use remote sensing based simulations as "ground truth" for calibration (Stisen et al., 2011; Zhang et al., 2009). This study calibrated the model parameters

15 using remote sensing snapshot (UAS) estimates of land surface variables such as T_s and SM.

Compared to complex land surface models, this approach is simple and efficient. It is especially suitable for operational applications to interpolate the remote sensing based snapshot estimates into the temporally continuous values. The practicality of the proposed approach for describing surface fluxes and water budgets in sites without flux stations and direct field observations. It can be used to estimate ecosystem states and flux exchange with the atmosphere for a larger part of a landscape

20 (e.g. farm) with temporally sparse UAS flight campaigns and online meteorological data. This has great potential to improve the management of agriculture ecosystems.

Both the look-up table and parameter optimization approaches were used in this study to obtain the parameter values. For instance, we used a look-up table (Carsel and Parrish, 1988) to get values of the fitting parameter of the Mualem model (n) and the infiltration rate for the saturated soil (K_s). The advantage of using the look-up table approach is that it can be easily

25 applied according to the site conditions, such as vegetation types, soil texture and soil depth. However, this approach requires prior knowledge on the site. Insufficient knowledge on the site conditions may lead to the selection of unsuitable parameter values from the look-up tables. For instance, K_s may vary at different soil layers and it could be difficult to select an effective K_s to represent the condition for the entire soil layers.

Regarding the optimization approach, this method has an advantage to achieve a good fitting performance with UAS

30 observations or estimates. However, this optimization approach needs to consider the number of observations and calibration parameters, parameter equifinality and multi-objective optimization (Her and Chaubey, 2015). For instance, due to limited fourteen UAS T_s or SM available for calibration, we selected only four parameters (C_{sat}, b, C_{veg}, and SWS_{max}), which are hard to obtain from the look-up table approach with insufficient prior knowledge of the site, for optimization. To deal with parameter

equifinality and multi-objective optimization, the Monte Carlo optimization was combined with the Pareto front analysis in this study. Other approaches e.g. Bayesian analysis could also be utilized to calibrate the model parameter with multiple objectives and separate the uncertainty sources: input, parameters and model structure (Vrugt et al., 2009). It can be a useful tool for the model calibration and quantification of the simulated uncertainty. Besides the look-up table and optimization

5 approaches, another promising approach is to estimate soil or plant hydraulic properties from imaging spectroscopy (Goldshleger et al., 2012; Nocita et al., 2015) or thermal imaging data (Jones, 2004).

5 Conclusion

Continuous estimation of land surface variables, such as surface temperature, net radiation, soil moisture, evapotranspiration and gross primary productivity at daily or monthly time scales is important for hydrological and ecological applications.

10 However, remotely sensed observations can be directly used to estimate the instantaneous status of land surface variables at the time of data acquisitions. Therefore, to continuously estimate land surface variables from remote sensing, this study developed a tool to fill the temporal gaps of land surface fluxes between data acquisitions and interpolate instantaneous estimates into continuous records. The tool is a dynamic Soil Vegetation Atmosphere Transfer model, the Soil-Vegetation, Energy, water and CO_2 traNsfer model (SVEN), which is a parsimonious model to continuously simulate land surface variables

15 with meteorological forcing and vegetation indices as model forcing. To interpolate the snapshot estimates from UAS, this study conducted the model parameter calibration to integrate the SVEN model and the snapshot estimates of surface temperature and soil moisture at the time of flight. This provides an effective way to continuously estimate land surface fluxes from remotely sensed observations. A case study was conducted with seven temporally sparse observations from UAS multispectral and thermal sensors in a Danish willow bioenergy plantation (DK-RCW) during the growing season of 2016

20 (180 days). Satisfactory results were achieved with the root mean square deviations for the simulated daily land surface temperature, net radiation, soil moisture, latent heat flux and gross primary productivity equal to 2.35 °C, 14.49 W·m^{-2}, 1.98% m^3·m^{-3}, 16.62 W·m^{-2} and 3.01 g·C·m^{-2}·d^{-1}, respectively.

This model based interpolation method has potential not just with UAS but also with remotely sensed data from other platforms, e.g. satellite and manned airborne systems, for a range of spatial and temporal scales. Additionally, the combination

25 of the model based interpolation approach and remotely sensed observations (e.g. Sentinel or MODIS land surface temperature and GPP products) can facilitate our understanding on the temporal upscaling of instantaneous estimates to the daily or longer time scales to improve our knowledge of the coupled energy, water and carbon cycles at various temporal scales.

30 *Data and code availability.* The data and code used in this study are available upon request from the corresponding authors.

Supplement. The supplement related to this article is available online.

Author contribution. All authors contributed to the design of this study and the model development. MG and PBG contributed to funding acquisition. AI made contributions to the eddy covariance and meteorological data. SW conducted the model simulation and UAV data collection. SW wrote the original draft. All authors contributed to the discussion of the results and the revision of this paper.

5   *Competing interests.* The authors declare that they have no conflict of interest.

Acknowledgement: The authors would like to thank the EU and Innovation Fund Denmark (IFD) for funding, in the frame of the collaborative international consortium AgWIT financed under the ERA-NET Co-fund Water Works 2015 Call. This ERA-NET is an integral part of the 2016 Joint Activities developed by the Water Challenges for a Changing World Joint Programme Initiative (Water JPI). This study was also supported by the Smart UAV project from IFD [125-2013-5]. SW was financed
10 from an internal PhD grant from the Department of Environmental Engineering at DTU and was financed by the COST action OPTIMISE for a short-term research stage.

References

Alfieri, J. G., Anderson, M. C., Kustas, W. P. and Cammalleri, C.: Effect of the revisit interval and temporal upscaling methods on the accuracy of remotely sensed evapotranspiration estimates, Hydrol. Earth Syst. Sci., 21(1), 83–98, doi:10.5194/hess-21-
15 83-2017, 2017.

Berni, J., Zarco-Tejada, P. J., Suarez, L. and Fereres, E.: Thermal and Narrowband Multispectral Remote Sensing for Vegetation Monitoring From an Unmanned Aerial Vehicle, IEEE Trans. Geosci. Remote Sens., 47(3), 722–738, doi:10.1109/TGRS.2008.2010457, 2009.

Boegh, E., Poulsen, R. N., Butts, M., Abrahamsen, P., Dellwik, E., Hansen, S., Hasager, C. B., Ibrom, A., Loerup, J. K.,
20 Pilegaard, K. and Soegaard, H.: Remote sensing based evapotranspiration and runoff modeling of agricultural, forest and urban flux sites in Denmark: From field to macro-scale, J. Hydrol., 377(3–4), 300–316, doi:10.1016/j.jhydrol.2009.08.029, 2009.

Brutsaert, W.: Evaporation into the Atmosphere. Theory, History, and Applications; Dordrecht: Holland, D, Reidel Co, 1982.

Calvet, J.-C., Noilhan, J. and Bessemoulin, P.: Retrieving the Root-Zone Soil Moisture from Surface Soil Moisture or Temperature Estimates: A Feasibility Study Based on Field Measurements, J. Appl. Meteorol., doi:10.1175/1520-
25 0450(1998)037<0371:RTRZSM>2.0.CO;2, 1998.

Carlson, T. N., Gillies, R. R. and Schmugge, T. J.: An interpretation of methodologies for indirect measurement of soil water content, Agric. For. Meteorol., 77(3–4), 191–205, doi:10.1016/0168-1923(95)02261-U, 1995.

Carsel, R. F. and Parrish, R. S.: Developing joint probability distributions of soil water retention characteristics, Water Resour. Res., 24(5), 755–769, doi:10.1029/WR024i005p00755, 1988.

30 Catmull, E. and Rom, R.: A CLASS OF LOCAL INTERPOLATING SPLINES, in Computer Aided Geometric Design., 1974.

Chen, Y., Xia, J., Liang, S., Feng, J., Fisher, J. B., Li, X., Li, X., Liu, S., Ma, Z., Miyata, A., Mu, Q., Sun, L., Tang, J., Wang,

K., Wen, J., Xue, Y., Yu, G., Zha, T., Zhang, L., Zhang, Q., Zhao, T., Zhao, L. and Yuan, W.: Comparison of satellite-based evapotranspiration models over terrestrial ecosystems in China, Remote Sens. Environ., 140, 279–293, doi:10.1016/j.rse.2013.08.045, 2014.

Choudhury, B. J. and Monteith, J. L.: A four-layer model for the heat budget of homogeneous land surfaces, Q. J. R. Meteorol. Soc., 114(480), 373–398, doi:10.1002/qj.49711448006, 1988.

Denis, G., Claverie, A., Pasco, X., Darnis, J. P., de Maupeou, B., Lafaye, M. and Morel, E.: Towards disruptions in Earth observation? New Earth Observation systems and markets evolution: Possible scenarios and impacts, Acta Astronaut., 137, 415–433, doi:10.1016/j.actaastro.2017.04.034, 2017.

Dettmann, U., Bechtold, M., Frahm, E. and Tiemeyer, B.: On the applicability of unimodal and bimodal van Genuchten-Mualem based models to peat and other organic soils under evaporation conditions, J. Hydrol., 515, 103–115, doi:10.1016/j.jhydrol.2014.04.047, 2014.

Djamai, N., Magagi, R., Goïta, K., Merlin, O., Kerr, Y. and Roy, A.: A combination of DISPATCH downscaling algorithm with CLASS land surface scheme for soil moisture estimation at fine scale during cloudy days, Remote Sens. Environ., 184, 1–14, doi:10.1016/j.rse.2016.06.010, 2016.

Ershadi, A., McCabe, M. F., Evans, J. P., Chaney, N. W. and Wood, E. F.: Multi-site evaluation of terrestrial evaporation models using FLUXNET data, Agric. For. Meteorol., 187, 46–61, doi:10.1016/j.agrformet.2013.11.008, 2014.

Fisher, J. B., Tu, K. P. and Baldocchi, D. D.: Global estimates of the land-atmosphere water flux based on monthly AVHRR and ISLSCP-II data, validated at 16 FLUXNET sites, Remote Sens. Environ., 112(3), 901–919, doi:10.1016/j.rse.2007.06.025, 2008.

Fisher, J. B., Melton, F., Middleton, E., Hain, C., Anderson, M., Allen, R., McCabe, M. F., Hook, S., Baldocchi, D., Townsend, P. A., Kilic, A., Tu, K., Miralles, D. D., Perret, J., Lagouarde, J. P., Waliser, D., Purdy, A. J., French, A., Schimel, D., Famiglietti, J. S., Stephens, G. and Wood, E. F.: The future of evapotranspiration: Global requirements for ecosystem functioning, carbon and climate feedbacks, agricultural management, and water resources, Water Resour. Res., 53(4), 2618–2626, doi:10.1002/2016WR020175, 2017.

Fratini, G., Ibrom, A., Arriga, N., Burba, G. and Papale, D.: Relative humidity effects on water vapour fluxes measured with closed-path eddy-covariance systems with short sampling lines, Agric. For. Meteorol., 165, 53–63, doi:10.1016/j.agrformet.2012.05.018, 2012.

GAO, W.: Parameterization Of Subgrid-Scale Land-Surface Fluxes With Emphasis On Distributing Mean Atmospheric Forcing And Using Satellite-Derived Vegetation Index, J. Geophys. Res., 100(D7), 14305–14317, doi:Doi 10.1029/95jd01464, 1995.

García, M., Sandholt, I., Ceccato, P., Ridler, M., Mougin, E., Kergoat, L., Morillas, L., Timouk, F., Fensholt, R. and Domingo, F.: Actual evapotranspiration in drylands derived from in-situ and satellite data: Assessing biophysical constraints, Remote Sens. Environ., 131, 103–118, doi:10.1016/j.rse.2012.12.016, 2013.

Garratt, J. R. and Hicks, B. B.: Momentum, heat and water vapour transfer to and from natural and artificial surfaces, Q. J. R.

Meteorol. Soc., 99(422), 680–687, doi:10.1002/qj.49709942209, 1973.

Goldshleger, N., Chudnovsky, A. and Ben-Dor, E.: Using reflectance spectroscopy and artificial neural network to assess water infiltration rate into the soil profile, Appl. Environ. Soil Sci., doi:10.1155/2012/439567, 2012.

Van de Griend and M.Owe., A. A.: On the relationship between thermal emissivity\nand normalized vegetation index for natural surfaces, Int. J. Remote Sens., 14(6), 1119–1131, doi:10.1080/01431169308904400, 1993.

Her, Y. and Chaubey, I.: Impact of the numbers of observations and calibration parameters on equifinality, model performance, and output and parameter uncertainty, Hydrol. Process., doi:10.1002/hyp.10487, 2015.

Huang, F., Zhan, W., Duan, S. B., Ju, W. and Quan, J.: A generic framework for modeling diurnal land surface temperatures with remotely sensed thermal observations under clear sky, Remote Sens. Environ., 150, 140–151, doi:10.1016/j.rse.2014.04.022, 2014.

Huang, F., Zhan, W., Voogt, J., Hu, L., Wang, Z., Quan, J., Ju, W. and Guo, Z.: Temporal upscaling of surface urban heat island by incorporating an annual temperature cycle model: A tale of two cities, Remote Sens. Environ., 186, 1–12, doi:10.1016/j.rse.2016.08.009, 2016.

Huning, L. S. and Margulis, S. A.: Watershed modeling applications with a modular physically-based and spatially-distributed watershed educational toolbox, Environ. Model. Softw., doi:10.1016/j.envsoft.2015.02.008, 2015.

Ibrom, A., Dellwik, E., Flyvbjerg, H., Jensen, N. O. and Pilegaard, K.: Strong low-pass filtering effects on water vapour flux measurements with closed-path eddy correlation systems, Agric. For. Meteorol., 147(3–4), 140–156, doi:10.1016/j.agrformet.2007.07.007, 2007.

Jin, Y., Ge, Y., Wang, J. and Heuvelink, G. B. M.: Deriving temporally continuous soil moisture estimations at fine resolution by downscaling remotely sensed product, Int. J. Appl. Earth Obs. Geoinf., 68, 8–19, doi:10.1016/j.jag.2018.01.010, 2018.

Jones, H. G.: Application of Thermal Imaging and Infrared Sensing in Plant Physiology and Ecophysiology., 2004.

Jung, M., Reichstein, M., Margolis, H. A., Cescatti, A., Richardson, A. D., Arain, M. A., Arneth, A., Bernhofer, C., Bonal, D., Chen, J., Gianelle, D., Gobron, N., Kiely, G., Kutsch, W., Lasslop, G., Law, B. E., Lindroth, A., Merbold, L., Montagnani, L., Moors, E. J., Papale, D., Sottocornola, M., Vaccari, F. and Williams, C.: Global patterns of land-atmosphere fluxes of carbon dioxide, latent heat, and sensible heat derived from eddy covariance, satellite, and meteorological observations, J. Geophys. Res. Biogeosciences, 116(3), doi:10.1029/2010JG001566, 2011.

Malbéteau, Y., Merlin, O., Balsamo, G., Er-Raki, S., Khabba, S., Walker, J. P. and Jarlan, L.: Toward a Surface Soil Moisture Product at High Spatiotemporal Resolution: Temporally Interpolated, Spatially Disaggregated SMOS Data, J. Hydrometeorol., 19(1), 183–200, doi:10.1175/JHM-D-16-0280.1, 2018.

McCabe, M. F., Rodell, M., Alsdorf, D. E., Miralles, D. G., Uijlenhoet, R., Wagner, W., Lucieer, A., Houborg, R., Verhoest, N. E. C., Franz, T. E., Shi, J., Gao, H. and Wood, E. F.: The future of Earth observation in hydrology, Hydrol. Earth Syst. Sci., 21(7), 3879–3914, doi:10.5194/hess-21-3879-2017, 2017.

McCallum, I., Wagner, W., Schmullius, C., Shvidenko, A., Obersteiner, M., Fritz, S. and Nilsson, S.: Satellite-based terrestrial production efficiency modeling., Carbon Balance Manag., 4(1), 8, doi:10.1186/1750-0680-4-8, 2009.

Mercado, L. M., Bellouin, N., Sitch, S., Boucher, O., Huntingford, C., Wild, M. and Cox, P. M.: Impact of changes in diffuse radiation on the global land carbon sink., Nature, 458(7241), 1014–1017, doi:10.1038/nature07949, 2009.

Miralles, D. G., Jiménez, C., Jung, M., Michel, D., Ershadi, A., Mccabe, M. F., Hirschi, M., Martens, B., Dolman, A. J., Fisher, J. B., Mu, Q., Seneviratne, S. I., Wood, E. F. and Fernández-Prieto, D.: The WACMOS-ET project - Part 2: Evaluation of global terrestrial evaporation data sets, Hydrol. Earth Syst. Sci., 20(2), 823–842, doi:10.5194/hess-20-823-2016, 2016.

Monteith, J. L.: Solar Radiation and Productivity in Tropical Ecosystems, J. Appl. Ecol., 9(3), 747, doi:10.2307/2401901, 1972.

Mu, Q., Zhao, M. and Running, S. W.: MODIS Global Terrestrial Evapotranspiration (ET) Product (MOD16A2/A3) - ATBD Collection 5, , 66, 2013.

Mualem, Y.: New Model for Predicting Hydraulic Conductivity of Unsaturated Porous-Media, Water Resour. Res., 12(3), 513–522, doi:Doi 10.1029/Wr012i003p00513, 1976.

Nocita, M., Stevens, A., van Wesemael, B., Aitkenhead, M., Bachmann, M., Barthes, B., Dor, E. B., Brown, D. J., Clairotte, M., Csorba, A., Dardenne, P., DemattÃa, J. A., Genot, V., Guerrero, C., Knadel, M., Montanarella, L., Noon, C., Ramirez-Lopez, L. and Wetterlind, J.: Chapter Four - Soil Spectroscopy: An Alternative to Wet Chemistry for Soil Monitoring, Adv. Agron., 2015.

Noilhan, J. and Mahfouf, J. F.: The ISBA land surface parameterisation scheme, Glob. Planet. Change, 13(1–4), 145–159, doi:10.1016/0921-8181(95)00043-7, 1996.

Noilhan, J. and Planton, S.: A Simple Parameterization of Land Surface Processes for Meteorological Models, Mon. Weather Rev., 117(3), 536–549, doi:10.1175/1520-0493(1989)117<0536:ASPOLS>2.0.CO;2, 1989.

Pilegaard, K., Ibrom, A., Courtney, M. S., Hummelshøj, P. and Jensen, N. O.: Increasing net CO2 uptake by a Danish beech forest during the period from 1996 to 2009, Agric. For. Meteorol., 151(7), 934–946, doi:10.1016/j.agrformet.2011.02.013, 2011.

Potter, C. S., Randerson, J. T., Field, C. B., Matson, P. A., Vitousek, P. M., Mooney, H. A. and Klooster, S. A.: Terrestrial ecosystem production: A process model based on global satellite and surface data, Global Biogeochem. Cycles, 7(4), 811–841, doi:10.1029/93GB02725, 1993.

Priestley, C. and Taylor, R.: On the assessment of surface heat flux and evaporation using large-scale parameters, Mon. Weather Rev., (February), 81–92, doi:10.1175/1520-0493(1972)100<0081:OTAOSH>2.3.CO;2, 1972.

Reichstein, M., Falge, E., Baldocchi, D., Papale, D., Aubinet, M., Berbigier, P., Bernhofer, C., Buchmann, N., Gilmanov, T., Granier, A., Grünwald, T., Havránková, K., Ilvesniemi, H., Janous, D., Knohl, A., Laurila, T., Lohila, A., Loustau, D., Matteucci, G., Meyers, T., Miglietta, F., Ourcival, J. M., Pumpanen, J., Rambal, S., Rotenberg, E., Sanz, M., Tenhunen, J., Seufert, G., Vaccari, F., Vesala, T., Yakir, D. and Valentini, R.: On the separation of net ecosystem exchange into assimilation and ecosystem respiration: Review and improved algorithm, Glob. Chang. Biol., 11(9), 1424–1439, doi:10.1111/j.1365-2486.2005.001002.x, 2005.

Roderick, M. L., Farquhar, G. D., Berry, S. L. and Noble, I. R.: On the direct effect of clouds and atmospheric particles on the

productivity and structure of vegetation, Oecologia, 129(1), 21–30, doi:10.1007/s004420100760, 2001.

Running, S. W. and Coughlan, J. C.: A general model of forest ecosystem processes for regional applications I. Hydrologic balance, canopy gas exchange and primary production processes, Ecol. Modell., 42(2), 125–154, doi:10.1016/0304-3800(88)90112-3, 1988.

5 Running, S. W., Nemani, R. R., Heinsch, F. A. N. N., Zhao, M., Reeves, M. and Hashimoto, H.: A Continuous Satelite-lDerived Measure of Global Terrestrial Primary Production, Bioscience, 54(6), 547, doi:10.1641/0006-3568(2004)054, 2004.

Sandholt, I., Rasmussen, K. and Andersen, J.: A simple interpretation of the surface temperature/vegetation index space for assessment of surface moisture status, Remote Sens. Environ., 79(2–3), 213–224, doi:10.1016/S0034-4257(01)00274-7, 2002.

Sellers, P. J., Randall, D. A., Collatz, G. J., Berry, J. A., Field, C. B., Dazlich, D. A., Zhang, C., Collello, G. D. and Bounoua,
10 L.: A revised land surface parameterization (SiB2) for atmospheric GCMs. Part I: Model formulation, J. Clim., 9(4), 676–705, doi:10.1175/1520-0442(1996)009<0676:ARLSPF>2.0.CO;2, 1996.

Shuttleworth, W. J. and Wallace, J. S.: Evaporation from sparse crops-an energy combination theory, Q. J. R. Meteorol. Soc., 111(465), 839–855, doi:10.1002/qj.49711146510, 1985.

Stisen, S., McCabe, M. F., Refsgaard, J. C., Lerer, S. and Butts, M. B.: Model parameter analysis using remotely sensed pattern
15 information in a multi-constraint framework, J. Hydrol., doi:10.1016/j.jhydrol.2011.08.030, 2011.

Twine, T. E., Kustas, W. P., Norman, J. M., Cook, D. R., Houser, P. R., Meyers, T. P., Prueger, J. H., Starks, P. J. and Wesely, M. L.: Correcting eddy-covariance flux underestimates over a grassland, Agric. For. Meteorol., 103(3), 279–300, doi:10.1016/S0168-1923(00)00123-4, 2000.

Vinukollu, R. K., Meynadier, R., Sheffield, J. and Wood, E. F.: Multi-model, multi-sensor estimates of global
20 evapotranspiration: climatology, uncertainties and trends, Hydrol. Process., 25(26), 3993–4010, doi:10.1002/hyp.8393, 2011.

Vrugt, J. A., ter Braak, C. J. F., Gupta, H. V. and Robinson, B. A.: Equifinality of formal (DREAM) and informal (GLUE) Bayesian approaches in hydrologic modeling?, Stoch. Environ. Res. Risk Assess., doi:10.1007/s00477-008-0274-y, 2009.

Wang, S., Ibrom, A., Bauer-Gottwein, P. and Garcia, M.: Incorporating diffuse radiation into a light use efficiency and evapotranspiration model: An 11-year study in a high latitude deciduous forest, Agric. For. Meteorol., 248(July), 479–493,
25 doi:10.1016/j.agrformet.2017.10.023, 2018a.

Wang, S., Garcia, M., Ibrom, A., Jakobsen, J., Josef Köppl, C., Mallick, K., Looms, M. and Bauer-Gottwein, P.: Mapping Root-Zone Soil Moisture Using a Temperature–Vegetation Triangle Approach with an Unmanned Aerial System: Incorporating Surface Roughness from Structure from Motion, Remote Sens., 10(12), 1978, 2018b.

Westermann, S., Langer, M. and Boike, J.: Spatial and temporal variations of summer surface temperatures of high-arctic
30 tundra on Svalbard - Implications for MODIS LST based permafrost monitoring, Remote Sens. Environ., 115(3), 908–922, doi:10.1016/j.rse.2010.11.018, 2011.

Wilson, K., Goldstein, A., Falge, E., Aubinet, M., Baldocchi, D., Berbigier, P., Bernhofer, C., Ceulemans, R., Dolman, H., Field, C., Grelle, A., Ibrom, A., Law, B. E., Kowalski, A., Meyers, T., Moncrieff, J., Monson, R., Oechel, W., Tenhunen, J., Valentini, R. and Verma, S.: Energy balance closure at FLUXNET sites, Agric. For. Meteorol., 113(1–4), 223–243,

doi:10.1016/S0168-1923(02)00109-0, 2002.

Wutzler, T., Lucas-Moffat, A., Migliavacca, M., Knauer, J., Sickel, K., Šigut, L., Menzer, O. and Reichstein, M.: Basic and extensible post-processing of eddy covariance flux data with REddyProc, Biogeosciences, 15(16), 5015–5030, doi:10.5194/bg-15-5015-2018, 2018.

5 Yapo, P. O., Gupta, H. V. and Sorooshian, S.: Multi-objective global optimization for hydrologic models, J. Hydrol., doi:10.1016/S0022-1694(97)00107-8, 1998.

Zhang, X., Pang, J. and Li, L.: Estimation of Land Surface temperature under cloudy skies using combined diurnal solar radiation and surface temperature evolution, Remote Sens., 7(1), 905–921, doi:10.3390/rs70100905, 2015.

Zhang, Y., Chiew, F. H. S., Zhang, L. and Li, H.: Use of remotely sensed actual evapotranspiration to improve rainfall-runoff
10 modeling in Southeast Australia, J. Hydrometeorol., doi:10.1175/2009JHM1061.1, 2009.